Progress In Electromagnetics Research, PIER 88, 275–287, 2008

SIGNAL MODEL ANALYSIS OF A 35GHZ ALTERNATING CURRENT DIRECT DETECTION RECEIVER

M.-H. Yang, F.-H. Guan, J. Xu, X. Shi, and X.-W. Sun †

Shanghai Institute of Microsystems and
Information Technology of CAS
Shanghai 200050, China

Abstract—A 35 GHz alternating current (AC) direct detection receiver for passive imaging has been studied and presented. The Monolithic Microwave Integrated Circuits (MMIC) Low Noise Amplifiers (LNAs) with high gain and wide band are cascaded to provide enough gain for high sensitivity in the receiver. On basic of discussing the structure and mechanical chopping modulation, the signal model and compensation mechanism is emphatically analyzed. Finally, the imaging result is given.

1. INTRODUCTION

Passive imaging at millimeter wavelengths has recently seen a surge of investment in both the government and commercial sectors. Passive millimeter wave imaging system can be used to obtain imaging information through clouds, dusts, flames, and other obstructions render visible systems ineffective. These applications which benefit from passive imaging are concealed weapons detections, aircraft landing aid in fog and all-weather driver assistance [1–9].

Different from the traditional DC direct detection receiver, the AC direct detection receiver obtains the information of target by adopting AC component and removing DC component. The advantages of the AC direct detection receiver are eliminating bias drift, low DC noise, short integration time and simple structure [10–12].

In this paper, the system structure is described in Section 2 on basic of the radiometric theory. Then according to the mechanical chopping modulation, the signal spectrum and compensation

† M.-H. Yang, F.-H. Guan, and J. Xu are also with Graduate School of CAS, Beijing 100039, China

mechanism are analyzed in Section 3. Finally, a ladder shape of metal sheet is imaged by the receiver. The results show that the Ka-band AC direct detection receiver presented in this paper can be used in passive imaging.

2. 35 GHZ AC DIRECT DETECTION RECEIVER

2.1. Radiometric Basic

Passive imaging in millimeter wave is based on the fact, that different materials exhibit different radiation temperatures T_B depending on its own temperature and their physical properties [13].

$$T_B = eT_O + \rho T_U + tT_E \tag{1}$$

where e is absorptive/emissive factor, ρ is reflective factor, t is transmittive factor, T_O is the physical temperature of the object, T_U is the environmental temperature, T_E is the background temperature. Metal is mainly reflecting environmental temperature ($e = 0$, $\rho = 1$) and fabric exhibits transmissions in the range of $t = 0.3, \ldots, 0.8$. Due to these properties metal and other objects can be detected. The receiver detects the relative power, forming a grey scale image of the scene in a manner similar to a standard optical camera. The receiver outputs are amplified, digitized, and processed to form image of scene. Several different approaches are being used pursued for a millimeter wave imaging solution. In this paper, a common approach, direct detection in Ka band, is described.

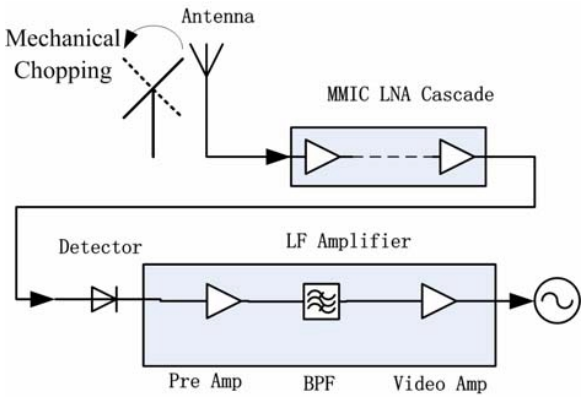

Figure 1. Block diagram of the imaging receiver.

2.2. Receiver Front-end

The schematic of passive imaging system based on the AC direct detection receiver is shown in Figure 1. The system includes mechanical chopping modulation and receiver front-end. The mechanical chopping modulates the input signal, which is similar to the way that the Dicke switch simply switches between the antenna and a calibrated noise source [14]. The mechanical chopping modulation will be described in Section 3. The whole system has only one single radiometric channel, mounted on a linear scanning system. The use of only one single receiver required a full two dimensional scan to image a scene.

As shown in Figure 1, the receiver front-end consists of a receiving antenna, a LNA cascade module, a detector and a low frequency (LF) amplifier. The horn antenna, which is sufficient for the requirement of spatial resolution, is adopted in the receiver. The other parts of the receiver front-end will be described in following paragraph.

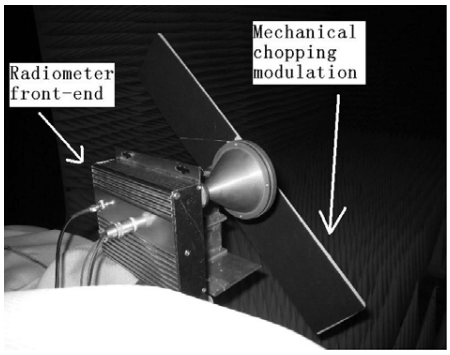

Figure 2. Photograph of imaging receiver.

2.3. LNA Cascade Module

For low cost and compactness, 0.25 μm GaAs PHEMT technology is used in LNA design. The MMIC LNA works in 26–38 GHz. The gain of the MMIC LNA is more than 18 dB, and the noise figure of that is less than 2.5 dB.

However, in direct detector receiver, the LNA gain must be high enough to effectively reduce the diode detector noise below the amplifier level.

The LNA gain can be estimated:

$$G_{RF} \geq \frac{P_{if}}{kT_{sy}BF_n} \tag{2}$$

where P_{if} is the minimum power input to the diode detector, T_{sy} is equivalent noise temperature of the system, B is equivalent RF bandwidth, F_n is system noise figure. For the receiver proposed in this paper, P_{if} is -35 dBm, which is determined by the curve of the detector's detected voltage power response. T_{sy} is 600 K, B is 6 GHz, and F_n is 3 dB. According to (2), G_{RF} should be more than 35 dB.

As only one LNA chip can not afford 35 dB gain, the LNA cascade module is adopted. The S-parameters of the LNA cascade module is shown in Figure 3.

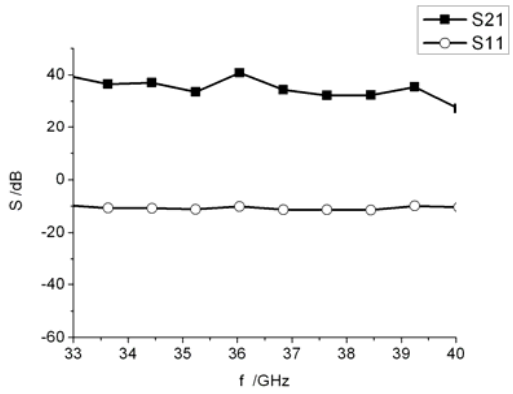

Figure 3. S parameters of LNA cascade module.

2.4. Detector

The detector is a zero bias square-law detection diode, hsch-9161, which provides low saturate current, and small series resistance.

Based on the small signal model, the detector circuit is designed, which consists of band-stop RF filter, π type match network and high resistance grounding microstrip line as DC path. The whole circuits are fabricated on RT/duroid 5880 dielectric material. The most important parameter of the detector is the voltage power response, which determines the working range of square-law detection, is measured and shown in Figure 4.

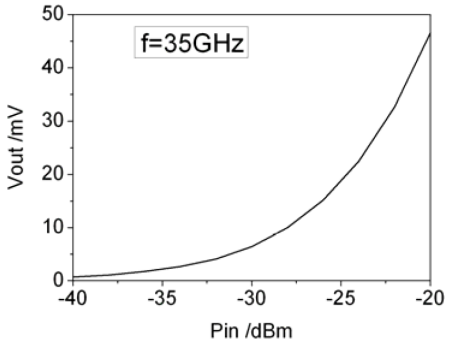

Figure 4. Voltage power response of the detector.

3. SIGNAL SPECTRUM AND COMPENSATION MECHANISM

As shown in Figure 2, the mechanical chopping modulation is realized by a "fan" with two vanes. The vanes are covered with microwave absorbing material as a calibrated source. If the fan is driven by a motor, the vanes will cut the beam of the antenna. The differential temperature comparison between the scene and the microwave absorbing material is realized. The effect of mechanical chopping modulation is the same as the Dicke switch switching between the scene and calibrated noise source, which can eliminate the bias drift (e.g., $1/f$ noise) [15].

The antenna temperature T_A can be expressed as [16, 17]:

$$T_A = \frac{1}{4\pi} \iint_{4\pi} T_i(\theta, \phi) G(\theta, \phi) d\Omega \tag{3}$$

where $T_i(\theta, \phi)$ is the temperature in the range of antenna beam, $G(\theta, \phi)$ is antenna radiation pattern.

Because the beam width of the antenna is $2\theta_{0.5E} = 2\theta_{0.5H} = 7.5^\circ$, the integration in (3) can be calculated in the projection round of the antenna beam.

Because the radiation pattern of horn antenna is rotational symmetry, $G(\theta, \phi)$ is independent of ϕ, and can be approximated to the following model:

$$G(\theta, \phi) = G_0 \exp\left(-b\theta^2\right) \tag{4}$$

where G_0 is the max gain of the antenna, b is the waveform coefficient of the antenna.

When the vanes don't cut the antenna beam, $T_i(\theta, \phi)$ is the temperature of scene in the range of the antenna beam, and is approximated to be a constant T_C. Thus T_A is also a constant.

$$T_A = T_{AC} = \frac{1}{4\pi} \iint_{4\pi} T_C G_0 \exp\left(-b\theta^2\right) d\Omega \tag{5}$$

The output of detector is direct voltage.

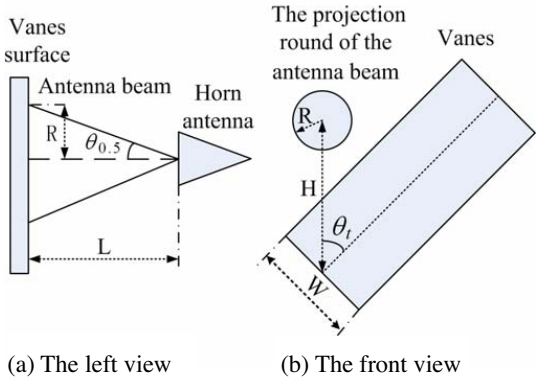

Figure 5. The position of the antenna and vanes.

When the vanes are cutting the antenna beam, $T_i(\theta, \phi)$ also consists of the temperature of the microwave absorbing material T_t. The beam solid angle which the vanes occupy is Ω_t. In this situation, T_A is:

$$\begin{aligned} T_A &= \frac{1}{4\pi} \iint_{4\pi} T_i(\theta, \phi) G_0 \exp\left(-b\theta^2\right) d\Omega \\ &= \frac{1}{4\pi} \left[\iint_{\Omega_t} T_t G_0 \exp\left(-b\theta^2\right) d\Omega + \iint_{4\pi - \Omega_t} T_C G_0 \exp\left(-b\theta^2\right) d\Omega \right] \\ &= \frac{1}{4\pi} \iint_{\Omega_t} \Delta T_{tc} G_0 \exp(-b\theta^2) d\Omega + T_{AC} \end{aligned} \tag{6}$$

where $\Delta T_{tc} = T_t - T_C$. As ΔT_{tc} is changing with time, the output of detector consists of alternating voltage when the vanes are cutting the antenna beam. Before analyzing the alternating component of T_A, some position parameters are defined and shown in Figure 5.

L is the distance between the antenna and vanes.

$\theta_{0.5}$ is half of the beam width.

R is the radius of the projection round of the antenna beam in vanes surface and $R = L * \mathrm{tg}\theta_{0.5}$.

H is the distance between the center of projection round and the center of the fan.

W is the width of the vanes and $W > 2R$.

The process of vanes cutting the antenna beam is shown in Figure 6.

In Figure 6, θ_1, θ_2 and θ_3 is:

$$\theta_1 = \arcsin\left(\frac{R + 0.5W}{H}\right), \quad \theta_2 = \arcsin\left(\frac{0.5W}{H}\right), \quad \theta_1 = \arcsin\left(\frac{0.5W - R}{H}\right) \tag{7}$$

According to the geometric relation of the vans and the projection round of the antenna beam in Figure 5 and Figure 6, T_A is calculated in (10)–(13). The integration of (10)–(13) is calculated in the projection round of the antenna beam.

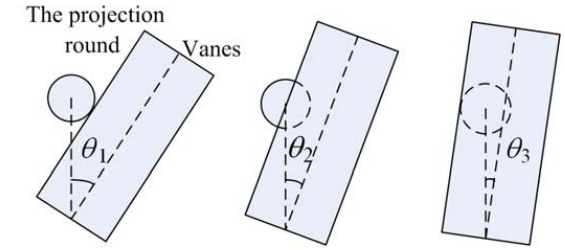

(a) The vane is tangent to the projection round

(b) The vane is occupying half of the projection round

(c) The vane is occupying the whole projection round

Figure 6. The process of vanes cutting the antenna beam.

When $\theta_1 < \theta_t < 0.5\pi$

$$T_A = T_{AC} \tag{8}$$

When $\theta_2 < \theta_t < \theta_1$

$$T_A = \frac{\Delta T_{AC} G_0}{4\pi} \times \int_0^{2\arccos\left[\frac{H\sin\theta_t - 0.5W}{R}\right]} \int_{H\sin\theta_t - 0.5W}^{R} \exp\left[-b\left(\mathrm{atg}\frac{l}{L}\right)^2\right] \times \sin\left[\mathrm{atg}\left(\frac{l}{L}\right)\right] d\left(\mathrm{atg}(\frac{l}{L})\right] d\phi + T_{AC} \tag{9}$$

When $\theta_3 < \theta_t < \theta_2$

$$T_A = T_{tC} - \frac{\Delta T_{AC} G_0}{4\pi} \times \int_0^{2\arccos\left[\frac{0.5W - H\sin\theta_t}{R}\right]} \int_{0.5W - H\sin\theta_t}^{R} \exp\left[-b\left(\mathrm{atg}\frac{l}{L}\right)^2\right] \times \sin\left[\mathrm{atg}\left(\frac{l}{L}\right)\right] d(\mathrm{atg}\left(\frac{l}{L}\right)\Big] d\phi \tag{10}$$

When $0 < \theta_t < \theta_3$

$$T_A = T_{tC} = \frac{1}{4\pi} \iint_{4\pi} T_t G_0 \exp\left(-b\theta^2\right) d\Omega \tag{11}$$

Because the beam width of the antenna is small ($2\theta_{0.5E} = 2\theta_{0.5H} = 7.5^\circ$), the approximate calculating formula (14) is used to simplify the integration in (8)–(11).

$$\mathrm{atg}\left(\frac{l}{L}\right) \approx \sin\left(\frac{l}{L}\right) \approx \sin\left(\mathrm{atg}\left(\frac{l}{L}\right)\right) \approx \frac{l}{L} \tag{12}$$

Finally, T_A can be expressed as following formula:
When $\theta_1 < \theta_t < 0.5\pi$

$$T_A = T_{AC} \approx \frac{T_C G_0}{4} \left\{1 - \exp\left[-b\left(\frac{R}{L}\right)^2\right]\right\} \tag{13}$$

When $\theta_2 < \theta_t < \theta_1$

$$T_A \approx \frac{\Delta T_{AC} G_0}{4\pi b} \times \arccos\left(\frac{H\sin\theta_t - 0.5W}{R}\right) \times \exp\left\{b\left[\left(\frac{R}{L}\right)^2 - \left(\frac{H\sin\theta_t - 0.5W}{L}\right)^2\right]\right\} + T_{AC} \tag{14}$$

When $\theta_3 < \theta_t < \theta_2$

$$T_A \approx T_C - \frac{\Delta T_{AC} G_0}{4\pi b} \times \arccos\left(\frac{0.5W - H\sin\theta_t}{R}\right) \times \exp\left\{b\left[\left(\frac{R}{L}\right)^2 - \left(\frac{0.5W - H\sin\theta_t}{L}\right)^2\right]\right\} \tag{15}$$

When $0 < \theta_t < \theta_3$

$$T_A = T_{tC} \approx \frac{T_t G_0}{4} \left\{1 - \exp\left[-b\left(\frac{R}{L}\right)^2\right]\right\} \tag{16}$$

If the rotational speed of the fan is f_m and θ_t verifies from 0.5π to 0, it's easy to get that:

$$\theta_t = \frac{\pi}{2} - \frac{t}{2\pi f_m}, \quad 0 < t < \frac{\pi^2}{f_m} \tag{17}$$

According to (13)–(17), if ΔT_{tc} is 10 K, the AC component of T_A in one period of mechanical chopping modulation is shown in Figure 7(a). The spectrum of T_A is shown in Figure 7(b).

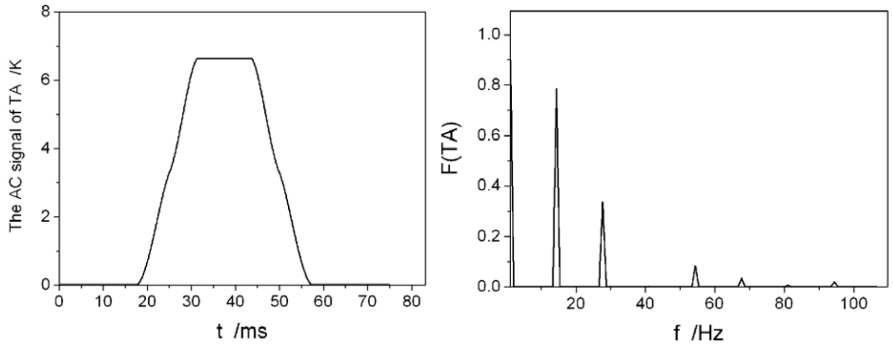

(a) The AC component of in one period (b) The spectrum of TA

Figure 7. The waveform and spectrum of T_A.

As shown in Figure 7(b), the DC component is the great proportion of the signal of T_A. However, in the AC receiver, the band-pass filter of LF amplifier should filter the DC component in order to eliminate the bias drift. In this situation, the output of receiver will be distorted. The real distorted signal is shown in Figure 8.

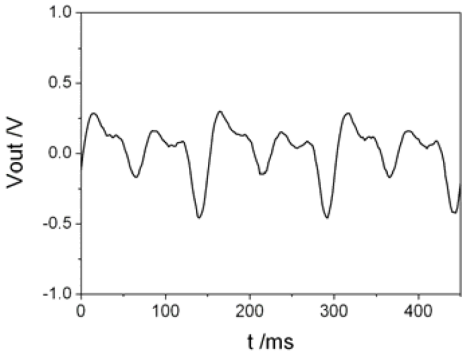

Figure 8. The distorted signal.

As shown in Figure 8, because of the distorted signal, it's difficult to accurately measure the relative power, which originates from ΔT_{tc}. Thus compensating the distorted signal is necessary.

Theoretically, the DC component which has been filtered out can not be restored excepted that some prior knowledge is given. However, as to the receiver presented in this paper, the signal model is given in (13)–(16). Thus the prior knowledge can be obtained from the signal model.

If the rotational speed of the fan is f_m, the power of distorted signal will center in f_m and $2f_m$, which is usually persevered by the band-pass filter of the video amplifier.

It's assumed that X is Fast Fourier Transforms (FFT) of the real distorted signal and X' is FFT of the theoretical signal which is shown in (13)–(16). As the DC component is filtered, it's easy to get the fact that:

$$X[0] \approx 0 \tag{18}$$

Theoretically, if $X[0]$ is not filtered, the ratio of $X[0]$ to $X[k_m]$ is equal to that of $X'[0]$ to $X'[k_m]$. Thus the DC component can be restored by the f_m component of the real distorted signal and theoretical signal model.

$$\frac{X[0]}{X[k_m]} = \frac{X'[0]}{X'[k_m]}, \quad k_m = \left|\frac{f_m}{f_s/N}\right| = \left|\frac{Nf_m}{f_s}\right| \tag{19}$$

where f_s is the sampling frequency of FFT, '||' stands for rounding function. The restored signal is shown in Figure 9.

Compared with the theoretical signal shown in Figure 7(a) and the restored signal shown in Figure 9, the restored signal is similar to

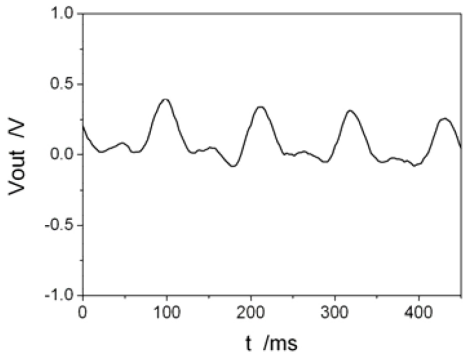

Figure 9. The restored signal.

the theoretical signal. Thus the relative power can be more accurately measured. However, because of some approximate conditions used in theoretical signal mode and some low frequency components not restored, the restored signal is still slightly distorted, which will decrease imaging quality.

4. EXPERIMENTAL RESULTS

The receiver is mounted on a linear scanning system to image a scene. The experiment was done with natural illumination through a window, which is more representative for indoor applications with a no coherent noise source illuminating the scene. The ladder metal is concealed behind the clothing as imaging target. The experiment scene and the radiometric image are shown in Figure 10.

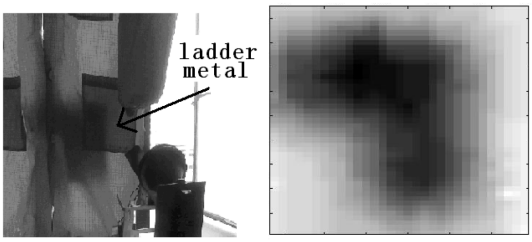

(a) experiment scene (b) radiometric image

Figure 10. The scene and result of passive imaging.

Although the beam width of the antenna is small, the spatial resolution is still not enough to make edge clear. In addition, the deficiency of the compensation mechanism analyzed in Section 3 is also the reason of edge blur effect. However, the outline of the radiometric image is close to the real ladder metal. Thus the receiver and the signal compensation mechanism can be used in passive imaging.

5. CONCLUSION

A 35 GHz AC direct detection receiver for a MMW passive imaging has been implemented. For the chopping mechanical modulation, the signal model is put forward. With the signal model as prior knowledge, a preliminary compensation mechanism is proposed. According to the result of the imaging experiment, it's demonstrated that the receiver can be used in MMW passive imaging. Our ongoing work is improving the compensation mechanism.

REFERENCES

1. Clark, S. E., J. A. Lovberg, C. A. Matiin, and V. Kolinko, "Passive millimeter-wave imaging for airborne and security application," *Proceedings for SPIE*, Vol. 5077, 16–27, 2003.
2. Oka, S., H. Togo, N. Kukutsu, and T. Nagatsuma, "Latest trends in millimeter-wave imaging technology," *PIER Letters*, Vol. 1, 197–204, 2008.
3. Guan, F. H., C. Wang, W. Z. Tian, R. Qian, and X. W. Sun, "Development of MMIC direct detection radiometers," *Journal of Infrared and Millimeter Waves*, Vol. 26, No. 02, 125–128, 2007.
4. Dou, W. B. and Z. L. Mei, "Electromagnetic analysis of symmetrical diffractive lens with small F-number and electrical large size," *Journal of Electromagnetic Waves and Applications*, Vol. 19, 1359–1374, 2005.
5. Chen, X., D. Liang, and K. Huang, "Microwave imaging 3-D buried objects using parallel genetic algorithm combined with FDTD technique," *Journal of Electromagnetic Waves and Applications*, Vol. 20, 1761–1774, 2006.
6. Chiang, C. T. and B. K. Chung, "High resolution 3-D imaging," *Journal of Electromagnetic Waves and Applications*, Vol. 19, 1267–1281, 2005.
7. Dou, W. B., X. D. Deng, and J. H. Pan, "Analysis of extending the field-of-view of reverse-microscope imaging system at millimeter-wavelengths," *Journal of Electromagnetic Waves and Applications*, Vol. 18, 469–479, 2004.
8. Karanasiou, I. S., N. K. Uzunoglu, and A. Garetsos, "Electromagnetic analysis of a non-invasive 3D passive microwave imaging system," *Journal of Electromagnetic Waves and Applications*, Vol. 18, 379–380, 2004.
9. Mei, Z. L. and W. B. Dou, "Analysis of focal field of small F-number imaging system at millimeter wavelength," *Journal of Electromagnetic Waves and Applications*, Vol. 16, 929–941, 2002.
10. Li, X. G., *Millimeter Wave Near Sensing Technique and Application*, Beijing National Defense Industry Publishing House, 1991.
11. Zhang, G. F., X. G. Li, and G. W. Lou, "Research on passive MMW imaging based on an alternating current radiometer," *Journal of Infrared and Millimeter Waves*, Vol. 26, No. 06, 461–464, 2007.
12. Lou, G. W. and X. G. Li, "Research on the 3 mm band alternating current radiometer," *Journal of Microwaves*, Vol. 16, No. 3, 295–

298, 2000.

13. Camps, A., J. Bará, F. Torres, and I. Corbella, "Extension of the clean technique to the microwave imaging of continuous thermal sources by means of aperture synthesis radiometers," *Journal of Electromagnetic Waves and Applications*, Vol. 12, 311–313, 1998.
14. Lynch, J. J., J. N. Schulman, and H. P. Moyer, "Low noise direct detection sensors for millimeter wave imaging," *Compound Semiconductor Integrated Circuit Symposium, 2006 IEEE*, 215–218, 2006.
15. Lynch, J. J., H. P. Moyer, and J. H. Schaffner, "Passive millimeter-wave imaging module with preamplifier zero-bias detection," *IEEE Transactions on Microwave Theory and Techniques*, Vol. 56, 1592–1600, 2008.
16. Gustrau, F. and D. Manteuffel, *EM Modeling of Antennas and RF Components for Wireless Communication Systems*, 23–42, Springer Berlin Heidelberg, 2006.
17. Jacobsen, S. and P. Stauffer, "Performance evaluation of various antenna configurations for microwave thermography during superficial hyperthermia," *Journal of Electromagnetic Waves and Applications*, Vol. 15, 111–134, 2001.